

UC Berkeley

UC Berkeley Previously Published Works

Title

Rapid and Efficient Arsenic Removal by Iron Electrocoagulation Enabled with in Situ Generation of Hydrogen Peroxide

Permalink

<https://escholarship.org/uc/item/9vk367m0>

Journal

Environmental Science and Technology, 54(10)

ISSN

0013-936X

Authors

Bandaru, Siva RS
van Genuchten, Case M
Kumar, Arkadeep
[et al.](#)

Publication Date

2020-05-19

DOI

10.1021/acs.est.0c00012

Peer reviewed

1 **Rapid and efficient arsenic**
2 **removal by iron**
3 **electrocoagulation enabled with**
4 **in-situ generation of hydrogen**
5 **peroxide**

6

7 Siva RS Bandaru[†], Case M. van Genuchten[‡], Arkadeep Kumar[§], Sara
8 Glade[†], Dana Hernandez[†], Mohit Nahata[†], Ashok Gadgil ^{†, §, *}

9

10 † Department of Civil and Environmental Engineering, University of
11 California, Berkeley, California 94720-1710, United States

12 ‡ Geologic Survey of Denmark and Greenland, 1350 Copenhagen K,
13 Denmark

14 § Energy Technologies Area, Lawrence Berkeley National Laboratory,
15 Berkeley, California 94720, United States

16

17

18

19

20

21

22 **Corresponding Author***

23 E-mail: ajgadgil@ibl.gov; Phone number: (510) 486-4651; Fax: (510)

24 486-5454

25

26 **Abstract**

27 Millions of people are exposed to toxic levels of dissolved arsenic
28 in groundwater used for drinking. Iron electrocoagulation (FeEC) has
29 been demonstrated as an effective technology to remove arsenic at an
30 affordable price. However, FeEC requires long operating times
31 (~hours) to remove dissolved arsenic due to inherent kinetics
32 limitations. Air cathode Assisted Iron Electrocoagulation (“ACAIE”)
33 overcomes this limitation by cathodically generating H₂O₂ in-situ. In
34 ACAIE operation, rapid oxidation of Fe(II) and complete oxidation and
35 removal of As(III) are achieved. We compare FeEC and ACAIE for
36 removing As(III) from an initial concentration of 1464 µg/L, aiming for a
37 final concentration of less than 4 µg/L. We demonstrate that at short
38 electrolysis times (0.5 minutes), i.e. high charge dosage rates (1200 C/
39 L/min), ACAIE consistently outperformed FeEC in bringing arsenic
40 levels to less than WHO-MCL of 10 µg/L. Using XRD and XAS data, we
41 conclusively show that poor arsenic removal in FeEC arises from
42 incomplete As(III) oxidation, ineffective Fe(II) oxidation and the

43 formation of Fe(II-III) (hydr)oxides at short electrolysis times (<20
44 minutes). Finally, we report successful ACAIE performance (retention
45 time 19 seconds) in removing dissolved arsenic from contaminated
46 groundwater in rural California.

47

48 **Introduction**

49 Toxic levels of arsenic in groundwater used for drinking is a
50 major public health concern for nearly 200 million people around the
51 world.^{1, 2} Chronic exposure to arsenic causes various types of internal
52 cancers, cardiovascular diseases and gangrenes, and low I.Q in
53 children.³⁻⁵ Resource poor communities are adversely impacted by
54 arsenic poisoning due to the lack of affordable and robust solutions.⁶⁻⁸
55 Recently, iron electrocoagulation (FeEC) has been demonstrated as an
56 effective, affordable, and robust method to remove arsenic from
57 groundwater both in the laboratory and in extended field trials.⁹⁻¹¹

58 In FeEC, a low-voltage direct current applied across low-carbon
59 steel plates immersed into an electrolyte promotes oxidation of Fe(0)
60 to Fe(II) on the Fe anode and reduction of $H_2O/H_{2(g)}$ on the Fe cathode.¹²
61 In-situ generated Fe(II) undergoes further oxidation by dissolved O_2
62 (DO) in the bulk solution to form insoluble Fe(III) (oxyhydr)oxides.¹² In
63 addition, reactive intermediates (i.e. *OH , $^*O_2^-$, Fe(IV)) generated during
64 oxidation of Fe(II) by O_2 oxidize As(III) to As(V), which is more easily
65 adsorbed than As(III).¹³⁻¹⁷ Recent studies report that the charge dosage
66 (CD, C/L), charge dosage rate (CDR, C/L/min) and O_2 recharge rate
67 affect arsenic removal in FeEC for a given electrolyte composition.¹⁸ At
68 a constant CD (C/L), efficient arsenic removal occurs at low CDR
69 because the Fe(II) generation rate becomes lower than the rate of
70 atmospheric O_2 influx into the solution.¹⁸ This allows complete

71 oxidation of dissolved Fe(II) to Fe(III) (oxyhydr)oxides and subsequent
72 removal of arsenic. At higher CDR, imbalance between the rates of
73 Fe(II) generation and O₂ dissolution can result in incomplete oxidation
74 of Fe(II) and formation of the Fe(II-III) (hydr)oxide, green rust, which
75 can be less effective at removing arsenic than Fe(III) precipitates.¹⁹⁻²¹
76 While operating FeEC at low CDR avoids the formation of undesirable
77 green rust in most solutions, low CDR also requires long treatment
78 times (~hours), unattractive for real world applications.

79 Recently, air diffusion cathodes (herein called “air cathodes”)
80 have been shown to generate H₂O₂ by cathodic reduction of O₂ diffused
81 from air.²²⁻²⁴ An air cathode comprises a porous carbon cloth with a
82 hydrophobic gas diffusion layer on the air-facing side and a catalyst
83 layer facing the electrolyte. Air cathodes have been shown to produce
84 H₂O₂ at nearly 100% Faradaic efficiency over a wide range of current
85 densities and charge dosage rates.^{25, 26} Therefore, replacing the Fe
86 cathode in FeEC, which typically generates H_{2(g)}, with an air cathode
87 (technique herein referred to as Air Cathode Assisted Iron
88 Electrocoagulation, or “ACAIE”) results in cathodic H₂O₂ formation. In-
89 situ generated H₂O₂ oxidizes Fe(II) at nearly 4 orders of magnitude
90 faster than O₂ and also produces higher stoichiometric yields of
91 selective reactive intermediates (Fe(IV)) compared to O₂, which
92 enhances the kinetics of As(III) oxidation and removal by orders of
93 magnitude.^{13, 27, 28} Processes similar to ACAIE have been reported in the

94 literature under different terms (e.g., electro-Fenton, peroxi-
95 coagulation, etc.) with applications that addressed mainly the removal
96 of persistent organic contaminants at acidic pH via OH radical
97 formation. Only a few studies have examined arsenic removal at
98 circum-neutral pH using ACAIE, but these studies investigated only low
99 CDR operating conditions (2.8 C/L/min) with electrolysis duration of 60
100 mins, which is prohibitively long for real world applications.^{29, 30} These
101 studies also did not examine the structure and arsenic uptake mode of
102 the solids formed in ACAIE, which are expected to be significantly
103 different than those from standard FeEC systems, owing to different
104 pathways and kinetics of their formation. Knowledge of the structure
105 and arsenic bonding mode of the solids formed by ACAIE over a wide
106 range of CDR is essential to predict the arsenic sorption reactivity and
107 colloidal stability of the Fe(III) precipitates and leaching of sorbed
108 arsenic, since the mobilization of arsenic from solids depends on its
109 sorption mode.^{19, 31, 32}

110 In this work, we investigated As(III) removal using FeEC and
111 ACAIE systems over a wide range of operating CDR (1.5 C/L/min to
112 1200 C/L/min), corresponding to a electrolysis times from 0.5 to 400
113 minutes and current densities from 0.8 to 156 mA/cm². These
114 operating parameters are relevant to decentralized (community scale)
115 and centralized (municipal utility scale) drinking water treatment
116 plants and span the range of parameters used in other industries

117 (inorganic and organic wastewater treatment).^{10, 30} We characterized
118 the reaction products in both systems by X-ray diffraction (XRD) and
119 synchrotron-based Fe and As K-edge X-ray absorption spectroscopy
120 (XAS). With these macroscopic and molecular-scale data, we show that
121 ACAIE substantially and consistently outperforms FeEC in removing
122 high concentrations of As(III) to below 4 µg/L as the electrolysis time
123 decreases from hours to minutes (i.e. as CDR increases from 1.5 to
124 >1000 C/L/min). Finally, we demonstrate the performance of a flow-
125 through ACAIE reactor operated at high CDR in a field test using
126 arsenic-contaminated groundwater in a rural community in California.
127 Our results suggest that ACAIE systems can be an attractive
128 alternative to conventional arsenic removal strategies for communities
129 that require rapid flow-through treatment of large volumes of arsenic-
130 contaminated water.

131 **2 Materials and methods**

132 **2.1 Laboratory scale electrochemical experiments**

133 **2.1.1 FeEC reactor**

134 FeEC experiments were conducted in 0.5 L glass beakers with
135 two parallel low-carbon steel plates (1006-1026 steel grade, McMaster-
136 CARR) separated by a non-conducting spacer (acrylic rectangular
137 sheet: 14 cm × 2.5 cm × 2.5 cm) immersed in the electrolyte. The
138 total submerged surface area of the steel plates in the FeEC
139 experiments was 46 cm² (7 cm X 6.5 cm). These plates were cleaned

140 with sandpaper until the surfaces were shiny and then rinsed with
141 deionized water before the experiments.

142 **2.1.2 ACAIE reactor**

143 Laboratory scale ACAIE experiments were performed in a
144 custom-built rectangular batch reactor open to the atmosphere and
145 fitted with a carbon-based air cathode (submerged surface area of 64
146 cm²) on one side of the reactor. The air cathodes were fabricated
147 according to Barazesh et al. (2015), with further descriptions in the
148 supporting information (SI).²⁶ A rectangular steel plate (submerged
149 surface area of 45 cm², 1006-1026 steel grade, McMaster-CARR)
150 served as the anode and was placed parallel to the air cathode. A non-
151 conducting spacer (acrylic rectangular sheet: 14 cm × 2.5 cm × 1.3
152 cm) maintained an inter-electrode distance of 2.5 cm for all ACAIE
153 experiments except for those at CDR of 1200 C/L/min, which were
154 performed at an electrode spacing of 0.7 cm. Images of the 0.5 L
155 ACAIE experimental setup are shown in Figure S1. The same air
156 cathode was used for a single set of charge dosage rate experiments
157 (5 total experiments at CDR of 1.5, 6, 60, 100 and 600 C/L/min). A new
158 air cathode was used to repeat these experiments once and another
159 new air cathode was used to repeat the same experiments a third
160 time. No significant difference in the H₂O₂ Faradaic efficiency of the air
161 cathodes was observed at the beginning and end of each set of
162 replicate experiments (Figure S10A, S10B, S10C).

163 **2.1.3 Electrolysis**

164 An external DC power supply operated in galvanostatic mode
165 delivered specified currents to each system. The total charge dosage
166 was 600 C/L (3.1 mM Fe by Faraday's law) unless otherwise specified,
167 which was selected based on the operating parameters of an existing
168 FeEC plant treating arsenic-contaminated groundwater in West Bengal,
169 India.^{10, 11} To examine the impact of a wide range of operating
170 conditions on arsenic removal, we varied the electrolysis time from 1
171 to 400 minutes, which corresponds to CDRs of 600 to 1.5 C/L/min. The
172 volume factor in C/L/min is the actual electrolyte volume being treated.
173 Herein, electrolyte volume and reactor volume are used
174 interchangeably. Additional experiments at an electrolysis time of 0.5
175 minutes (CDR of 1200 C/L/min) were performed only in the ACAIE
176 system to understand the effect of reduced electrode spacing on
177 arsenic removal and energy consumption.

178 **2.1.4 Electrolyte and measurement protocols**

179 Batches of freshly prepared synthetic Bangladesh groundwater
180 (SBGW, composition listed in Table S1) were used as the electrolyte in
181 all laboratory experiments, unless otherwise noted.^{14, 33, 34} SBGW was
182 prepared with reagent grade chemicals and is described further in the
183 SI. The initial pH of each experiment was adjusted to 7.0 by bubbling
184 CO_{2(g)} or by adding small volumes of 1.1 M HCl or 1 M NaOH. The
185 electrolyte was stirred (~550 rpm) with a magnetic stir plate during

186 electrolysis. At the end of electrolysis, unfiltered and filtered (0.45 μm
187 Nylon filter) samples were collected to measure total and dissolved
188 concentrations of constituents. Herein, the constituents measured in
189 the filtrate are referred to as “dissolved concentrations”. The initial and
190 final pH, DO and conductivity were measured using an Orion Star™
191 A329 meter. Dissolved arsenic and iron concentrations were measured
192 by ICP-MS (Agilent 7700) and the concentrations of total Fe, P, Ca, Mg
193 and Si in the initial electrolytes were measured by ICP-OES
194 (PerkinElmer 5300 DV). New air cathodes were characterized for H_2O_2
195 generation before use in ACAIE experiments (see SI for experimental
196 details). All laboratory experiments were performed in triplicates at
197 room temperature; error bars represent the standard deviation of the
198 measurements.

199 **2.2 Field scale ACAIE experiments**

200 Field experiments were performed with local arsenic-
201 contaminated groundwater at a farm in rural community in California
202 using a custom flow-through ACAIE reactor with high surface area
203 (FigureS2). The primary goal of this field trial was to test the
204 effectiveness of ACAIE at intermediate scales in some worst-case
205 scenario conditions (i.e. short retention times) and it was not our goal
206 to test this prototype over extended periods. In this ACAIE system, an
207 air cathode and low-carbon steel anode (1006-1026 steel grade,
208 McMaster-CARR), each with a submerged surface area of 400 cm^2 ,

209 were positioned at an inter-electrode spacing of 1 cm. A stainless-steel
210 mesh (316 stainless steel wire cloth, 20 x 20 mesh size, 0.07 cm
211 opening size, wire diameter 0.06 cm) was used on the air-facing side of
212 the air cathode to act as a current collector and provide mechanical
213 support. Additional mechanical support to the air cathode and
214 stainless-steel mesh assembly was provided by a 1.3 cm thick acrylic
215 sheet with holes to access air, as shown in Figure S2A. This system was
216 operated at a flow rate of 1.3 L/min and with a hydraulic retention time
217 of 19 seconds. The actual electrolyte volume or reactor volume of this
218 reactor was 0.4 L. The CD and CDR employed in the field were 233 C/L
219 and 750 C/L/min. Samples for total and dissolved concentrations were
220 collected every five minutes at the outlet. The experiment was stopped
221 after treating 100 L of arsenic-contaminated groundwater (250
222 equivalent reactor volumes). At the end of electrolysis, commercial
223 grade alum (5 mg/L as Al) was added as a coagulant to the 100 L of
224 treated water and allowed to flocculate for another 20 minutes. After
225 flocculation, samples for measurement of dissolved arsenic were
226 collected by filtering an aliquot of treated water through a 0.45 μm
227 filter.

228 **2.3 X-ray diffraction**

229 Experiments for XRD characterization were conducted using the
230 FeEC and ACAIE experimental setups described in sections 2.1.1 and
231 2.1.2, but a simple electrolyte (5 mM NaCl, 5 mM NaHCO₃, pH 7) was

232 used instead of SBGW. We used the simple electrolyte, which was free
233 of surface-poisoning oxyanions, to ensure that the solids formed were
234 crystalline enough for adequate characterization by XRD. For this
235 analysis, we focused primarily on distinguishing between pure Fe(III)
236 precipitates and mixed-valent Fe(II-III) (hydr)oxides. Fe precipitates for
237 XRD measurements were collected on a 0.1 μm filter using a vacuum
238 pump. Fe(II-III) (hydr)oxide samples were collected under nitrogen
239 atmosphere and a small amount ($\sim 1\text{mL}$) of glycerol was added to the
240 filtered solids to prevent Fe(II) oxidation by exposure to air.³⁵
241 Diffractograms were collected from 5° to 95° 2θ with a Bruker AXS D8
242 Discover GADDS X-ray diffractometer, using Co K- α radiation. To
243 facilitate comparison among samples with different crystallinity, we
244 report the diffractograms normalized by the highest intensity peak.

245 **2.4 X-ray absorption spectroscopy**

246 Fe and As K-edge X-ray absorption spectra were collected at
247 beam line 4-1 of the Stanford Synchrotron Radiation Lightsource (SSRL,
248 Menlo Park, USA). Fe K-edge spectra were recorded at room
249 temperature in transmission mode out to k of 13 \AA^{-1} using ion
250 chambers to measure I_0 and I_t . As K-edge spectra were recorded at
251 liquid nitrogen temperatures ($\approx 80 \text{ }^\circ\text{K}$) in fluorescence mode out to k of
252 13.5 or 14 \AA^{-1} using a Lytle detector. Individual spectra were aligned,
253 averaged, and background-subtracted using SixPack software³⁶
254 following standard methods described previously.³⁷ The EXAFS spectra

255 were extracted using k^3 -weighting and the As K-edge EXAFS spectra
256 were Fourier-transformed over the k -range 4 to 13 \AA^{-1} using a Kaiser-
257 Bessel window with dk of 3 \AA^{-1} . Additional details regarding the sample
258 preparation and data collection procedures are given in the SI.

259 **2.4.1 As K-edge XANES analysis**

260 The percentages of As(III) and As(V) in each sample were
261 quantified by linear combination fits (LCFs) of the As K-edge XANES
262 spectra using the SixPack software.³⁶ To minimize systematic errors
263 due to the selection of particular reference compounds, we performed
264 three sets of LCFs for each sample using three sets of As(III) and As(V)
265 adsorption reference spectra: As(III) and As(V) adsorbed to 2-line
266 ferrihydrite, magnetite and green rust. The details of the synthesis and
267 data collection of these reference spectra are described elsewhere.^{19, 38}
268 The XANES LCFs were performed over the range of 11860 to 11880 eV,
269 with negative percentages disallowed. Individual LCFs were not
270 constrained to sum the percentages of fit-derived As(III) and As(V) to
271 100. We report the As(III) and As(V) percentages in the samples as the
272 average and standard deviation of the three sets of LCFs.

273 **2.4.2 As K-edge EXAFS shell-by-shell fits**

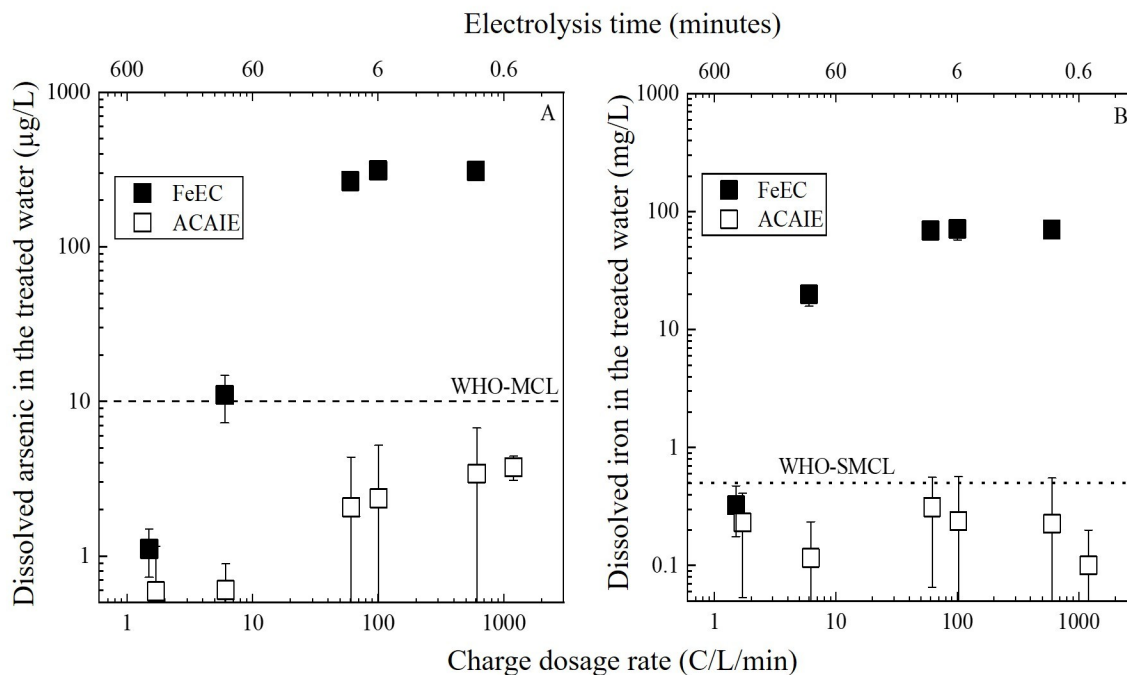
274 Theoretical curve fits of the As K-edge EXAFS spectra of select
275 samples and adsorption references were carried out in $R+\Delta R$ -space (\AA)
276 using the SixPack software,³⁶ which is built on algorithms derived from
277 the IFEFFIT library.³⁹ The presence of multiple arsenic oxidation states

278 bound to the solids can lead to the co-existence of several distinct
279 coordination complexes and multiple scattering paths, each with
280 different fitting parameters.⁴⁰ Therefore, to simplify our analysis, we
281 only performed shell-by-shell fits on samples determined by XANES
282 analysis to contain a single oxidation state (i.e. >90% As(III) or As(V)).
283 Phase and amplitude functions (As-O, As-O-O, As-Fe) were calculated
284 with FEFF6⁴¹ using the crystal structure of scorodite.⁴² We
285 geometrically constrained the As-O-O multiple-scattering path in the
286 fits to the first-shell As-O path and set its degeneracy to 12 for samples
287 containing As(V) and 6 for samples containing As(III). Further details of
288 the shell-by-shell fitting approach are given in the SI.

289 **3 Results**

290 **3.1 Behavior of bulk solution parameters in FeEC and ACAIE** 291 **systems**

292 **3.1.1 Arsenic removal**



293

294 Figure 1: Dissolved arsenic (A) and iron (B) remaining in the filtered
295 solution after electrolysis as a function of CDR in the FeEC (black
296 squares) and ACAIE (white squares) systems. The corresponding
297 electrolysis times are shown in the secondary X-axis above (note
298 decreasing values from left to right). The total charge dosage in each
299 experiment was 600 C/L. Synthetic Bangladesh groundwater was used
300 as the electrolyte (initial As(III) of $1464 \pm 83 \mu\text{g/L}$).
301
302

301

302

303

Figure 1A shows the effect of CDR on the residual arsenic in
304 solution after treatment in the FeEC and ACAIE systems for a total
305 charge dose of 600 C/L (3.1 mM Fe by Faraday's law). In the FeEC
306 system, the residual arsenic was less than 10 µg/L at the lowest CDR of
307 1.5 C/L/min, but increased to slightly more than 10 µg/L as the CDR
308 increased to 6 C/L/min. Dissolved arsenic levels after treatment
309 increased substantially when the CDR was increased further, leading to
310 20 times more aqueous arsenic ($>200 \mu\text{g/L}$) for all FeEC experiments

311 at CDR >6 C/L/min. Aqueous arsenic in the treated water in the FeEC
312 system was never below 300 $\mu\text{g/L}$ in experiments at the highest CDRs
313 of 100 to 600 C/L/min. In sharp contrast, the residual arsenic levels in
314 the ACAIE experiments depended less on CDR and were below 4 $\mu\text{g/L}$
315 for all experiments (white squares in Figure 1A). In ACAIE experiments,
316 dissolved arsenic in the treated water increased slightly from 0.6 ± 0.6
317 $\mu\text{g/L}$ to 3.8 ± 0.7 $\mu\text{g/L}$ across the entire range of CDRs from 1.5 to 1200
318 C/L/min, which corresponds to electrolysis times ranging from 400 to
319 0.5 minutes.

320 Figure 1B shows the influence of CDR on the dissolved iron
321 concentration immediately after electrolysis in the FeEC and ACAIE
322 systems. For FeEC experiments, the dissolved iron concentration
323 increased from 0.3 mg/L to 20 mg/L with an increase in CDR from 1.5
324 to 6 C/L/min, but then stabilized at 70 mg/L at CDR \geq 60 C/L/min. The
325 aqueous iron levels were also significantly lower using an air cathode
326 compared to an Fe cathode. In all ACAIE experiments, regardless of
327 CDR, the dissolved iron remained below the WHO Secondary MCL
328 (WHO-SMCL) of 0.3 mg/L.

329 **3.1.2 pH and DO**

330 The average initial pH in both FeEC and ACAIE experiments was
331 7.0 ± 0.1 . The final pH in FeEC and ACAIE experiments behaved
332 differently with CDR. The final pH in all FeEC experiments was always
333 at least 0.5 log units higher than the initial value and ranged from 7.6

334 to 7.9 (Figure S3A). In ACAIE experiments, the final pH also increased
335 from the initial value, but a more systematic trend with CDR was
336 observed. At the lowest CDR of 1.5 C/L/min, the final pH was 7.8,
337 whereas the final pH was only 7.1 at the highest CDR of 1200 C/L/min,
338 which corresponds to the shortest electrolysis time of 0.5 minutes.

339 The average initial DO in FeEC and ACAIE experiments was $7.4 \pm$
340 1.0 mg/L. The behavior of final DO differed significantly in the FeEC
341 and ACAIE experiments (Figure S3B). In the FeEC system, the DO
342 decreased substantially after treatment. The final DO was 3.5 mg/L
343 when the CDR was 1.5 C/L/min, and it decreased further as CDR
344 increased, leading to a DO of <0.1 mg/L for experiments at $CDR \geq 6$ C/
345 L/min. In contrast, the final DO in the ACAIE system was higher than
346 the initial value. The final DO increased from 8.7 to 11.7 mg/L with an
347 increase in CDR from 1.5 to 100 C/L/min, but dropped to 8.8 and 7.9
348 mg/L at CDR of 600 and 1200 C/L/min.

349 **3.1.3 Color and total iron concentrations of the suspension**

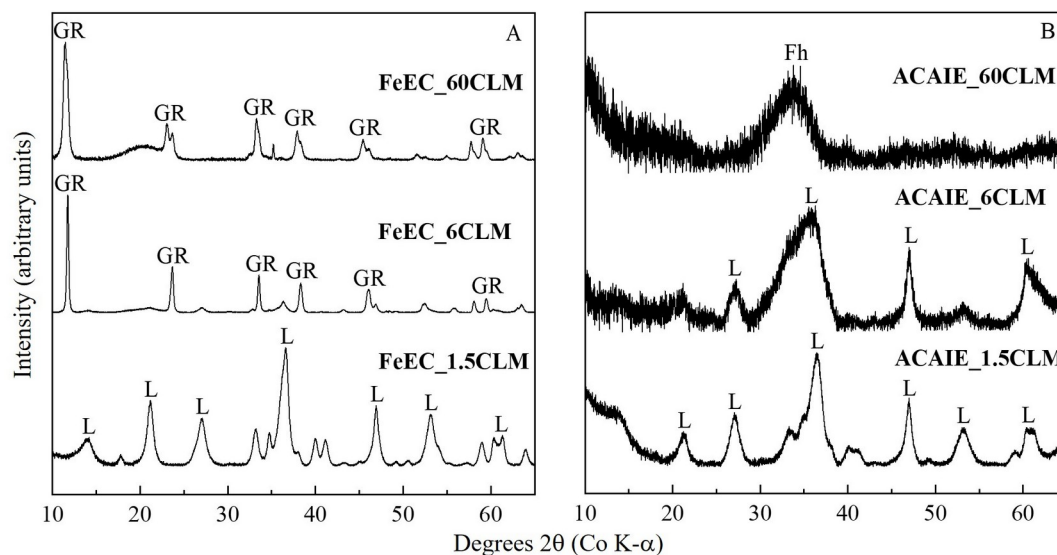
350 After electrolysis, visual inspection the electrolyte in FeEC
351 experiments showed orange precipitates at CDR of 1.5 C/L/min,
352 consistent with Fe(III) (oxyhydr)oxides, and the characteristic green-ish
353 blue color of green rust (GR) for experiments at $CDR \geq 6$ C/L/min
354 (Figure S4). Measurements of total iron in suspension indicated the
355 total iron produced was more than 90% of the theoretical value based
356 on Faraday's law at all CDRs except at 1.5 C/L/min, where only 82% of

357 the theoretical iron concentration was observed. In contrast to FeEC
358 experiments, only orange precipitates were observed in the ACAIE
359 system at all CDRs. Furthermore, the total iron measured in the ACAIE
360 experiments was >95% of the theoretical value at all CDRs (Figure S5).

361 The efficiency of H₂O₂ production by the air cathodes used in the
362 ACAIE experiments (Figure S6) was lowest at the lowest CDR of 1.5
363 C/L/min (48 ± 9% of the theoretical value), but increased steadily with
364 increasing CDR (>80% of the theoretical H₂O₂ at CDR > 60 C/L/min).

365 **3.2 Structure of iron precipitates formed in FeEC and ACAIE** 366 **systems**

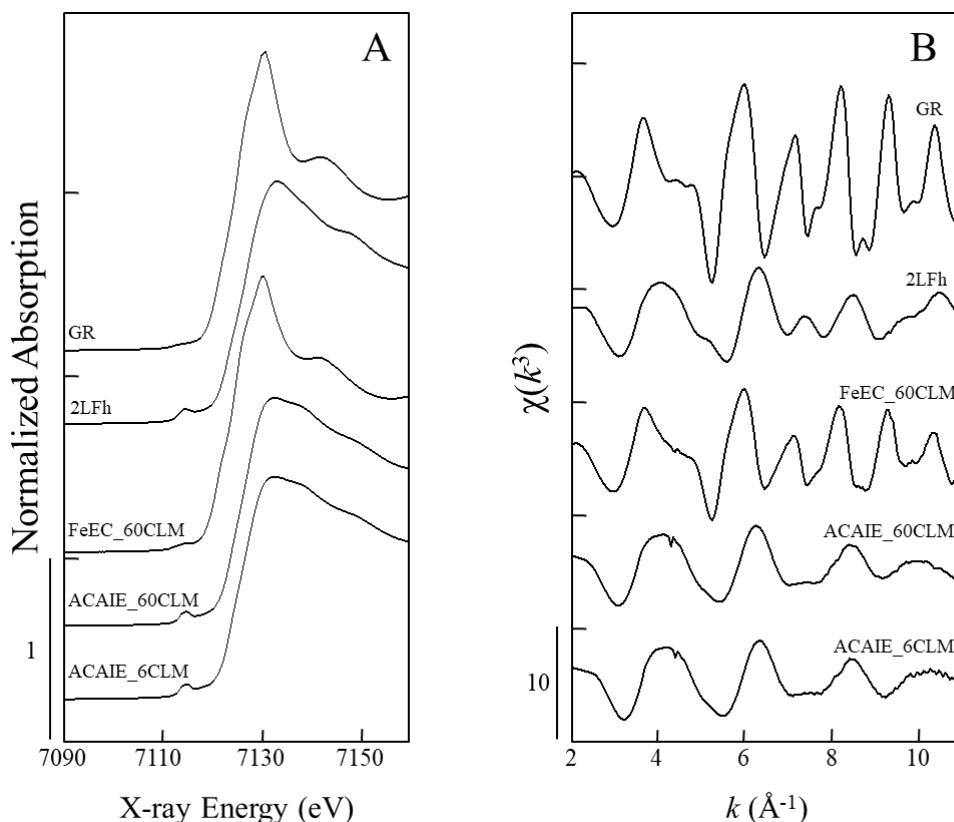
367 **3.2.1 X-ray diffraction**



368
369 Figure 2: XRD patterns of the Fe precipitates collected after electrolysis
370 in FeEC (A) and ACAIE (B) systems. The electrolyte was 5 mM NaCl + 5
371 mM NaHCO₃ (pH 7). The letters L, Fh and GR indicate the diffraction
372 peaks of lepidocrocite, ferrihydrite and carbonate green rust
373 respectively.⁴³⁻⁴⁶ CLM in the figures represents C/L/min. The broad peak
374 near 21° 2θ in Figure 2A arises from glycerol.
375

376 The diffractograms of the Fe precipitates in the FeEC and ACAIE
377 systems showed different characteristic Bragg peaks depending on
378 CDR (Figure 2). At low CDR, diffraction peaks from lepidocrocite were
379 observed in the FeEC system, consistent with the orange color of the
380 solids. However, as the CDR increased to 6 and 60 C/L/min,
381 characteristic Bragg peaks of carbonate GR were observed in the
382 solids, with intense reflections near $12^\circ 2\theta$ and $24^\circ 2\theta$. In addition, the
383 GR formed at 60 C/L/min had broader peaks than the 6 C/L/min
384 sample, consistent with its 10-fold shorter synthesis time. The XRD
385 patterns of the solids formed in the ACAIE experiments showed
386 systematic trends with CDR, but the changes in peak position and
387 intensity were different than those in the FeEC system. At CDR of 1.5
388 C/L/min, peaks consistent with lepidocrocite were observed, but the
389 peaks were broader than those at the same CDR in the FeEC system.
390 As the CDR increased from 1.5 to 60 C/L/min in the ACAIE system, the
391 diffraction patterns showed a progressive decrease in peaks arising
392 from lepidocrocite to peaks consistent with 2-line ferrihydrite (2LFh).
393 Similar to the FeEC system, the highest CDR in the ACAIE system
394 formed solids with the lowest crystallinity, but no evidence for mixed-
395 valent Fe(II-III) (hydr)oxides were observed.

396 **3.2.2 Fe K-edge XANES and EXAFS**



397
398 Figure 3: Fe K-edge XANES (A) and EXAFS spectra (B) of the Fe
399 precipitates formed in FeEC and ACAIE systems. Reference spectra for
400 green rust (GR) and 2-line ferrihydrite (2LFh) are also give for
401 comparison. SBGW was used as the electrolyte in these experiments.
402 CLM represents C/L/min.

403

404

405

The Fe K-edge XANES and EXAFS spectra of the Fe precipitates
406 formed in FeEC and ACAIE systems are compared to the spectra of Fe-
407 bearing reference minerals (e.g. GR and 2LFh) in Figure 3. Consistent
408 with the XRD data, the line shape of the XANES spectrum of solids
409 produced at 60 C/L/min in the FeEC system matched the GR reference
410 spectrum (Figure 3A), particularly the sharp absorption peak near 7130
411 eV. In addition, the EXAFS spectrum of this sample resembled the
412 EXAFS spectrum of GR, including the asymmetric first oscillation from

413 2.5 to 4.5 Å⁻¹. However, the EXAFS oscillations of the FeEC 60 C/L/min
414 sample had lower amplitude and were more broad than the GR
415 reference spectrum, which can be explained by the FeEC sample
416 having lower crystallinity than the reference GR due to its rapid
417 synthesis time and formation in the presence of surface-poisoning ions.

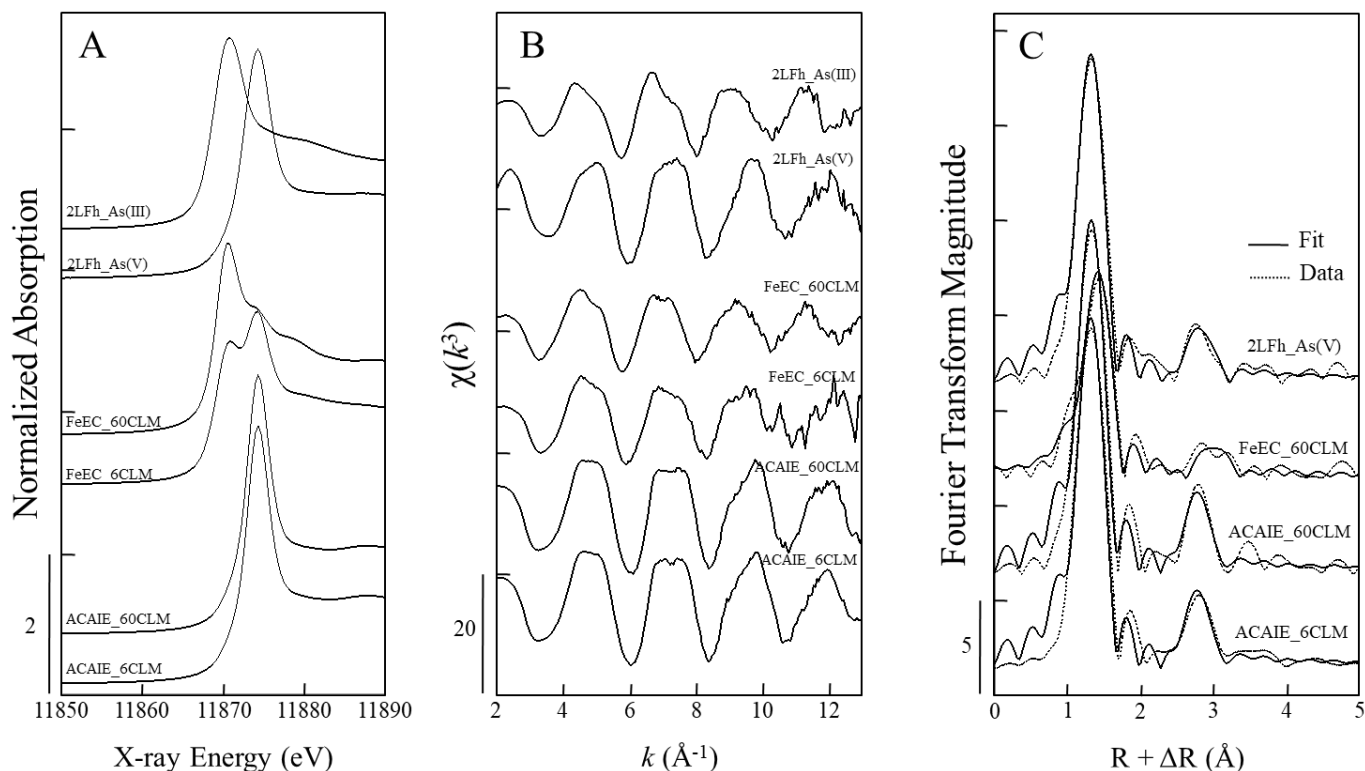
418 In contrast to the FeEC system, the ACAIE samples (6 and 60 C/L/
419 min) yielded solids with XANES spectra that matched closely that of
420 2LFh. The more intense pre-edge peak and the flattened region near
421 the absorption maximum, which is also found in the spectrum of 2LFh,
422 indicate the predominance of Fe(III) in the ACAIE samples, consistent
423 with the XRD patterns. The EXAFS spectra of the ACAIE samples also
424 matched that of 2LFh, particularly the symmetric first oscillation and
425 low amplitude peaks at $k > 8$ Å⁻¹. However, some subtle differences are
426 apparent between the EXAFS spectra of 2LFh and the ACAIE samples.
427 For example, the small shoulder in the first oscillation near 5.5 Å⁻¹ in
428 the 2LFh EXAFS spectrum is reduced in the ACAIE samples and the
429 small peak near 7.5 Å⁻¹ is flat in the ACAIE samples. These differences
430 are consistent with a lower degree of edge- and corner-sharing
431 bonding in the ACAIE samples relative to 2LFh.⁴⁷

432

433 **3.3 As X-edge X-ray absorption spectroscopy**

434 **3.3.1 As K-edge XANES spectra**

435



436

437 Figure 4: As K-edge XANES (A), EXAFS (B), and corresponding Fourier
438 transforms (C) of FeEC and ACAIE samples. Reference spectra of As(III)
439 and As(V) adsorbed to 2-line ferrihydrite (2LFh_As(III), 2LFh_As(V)) are
440 also given. In C), the shell-by-shell fitting output is given in solid lines
441 and the data is given in dotted lines. SBGW was used as the
442 electrolyte in these experiments. CLM represents C/L/min.
443

444 Figure 4A compares the As K-edge XANES spectra of solids
445 formed in the FeEC and ACAIE systems at CDRs of 6 and 60 C/L/min to
446 the reference spectra of As(III) and As(V) adsorbed to 2LFh. In the FeEC
447 system, the XANES spectrum of the solids formed at 6 C/L/min has two
448 distinct peaks with maxima near 11870 eV and 11874 eV, consistent
449 with the absorption maxima for the reference As(III) and As(V) spectra.
450 At increased CDR in the FeEC system, the peak indicative of As(III)
451 increases and is accompanied by a nearly complete decrease in the

452 As(V) peak. The LCFs of these samples (Table S2) confirm that the
453 As(III) percentage increases from $63 \pm 2\%$ to $100 \pm 2\%$ as the CDR
454 increases from 6 to 60 C/L/min, indicating inefficient As(III) oxidation at
455 high CDR in the FeEC system. By contrast, only peaks for As(V) are
456 apparent in the XANES spectra of samples produced at identical CDRs
457 of 6 and 60 C/L/min in the ACAIE system. The LCFs of the ACAIE
458 samples revealed a negligible percentage of As(III), with only As(V)
459 detected, which indicates highly effective As(III) oxidation using an air
460 cathode, even at high CDR values.

461 **3.3.2 As K-edge EXAFS spectra**

462 Figure 4B displays the As K-edge EXAFS spectra of samples
463 produced at CDR of 6 and 60 C/L/min in the FeEC and ACAIE systems.
464 In the FeEC system, the EXAFS oscillations of the samples resembled
465 the As(III) adsorption reference spectrum, consistent with the XANES
466 LCFs indicating the predominance of sorbed As(III). The first two
467 oscillations from 4 to 8 \AA^{-1} in the FeEC samples showed a small,
468 asymmetric shoulder at higher k , which is also present in the As(III)
469 adsorption reference. The EXAFS spectra of samples in the ACAIE
470 system are characterized by flatter oscillations from 4 to 8 \AA^{-1} than the
471 FeEC samples and the reference spectra. Compared to the reference
472 spectra, the ACAIE samples are a closer match to As(V) adsorbed to
473 2LFh, which is consistent with the absence of As(III) determined by
474 XANES LCFs.

475 **3.3.3 Shell-by-shell fits of the As K-edge EXAFS Spectra**

476 Figure 4C shows the Fourier-transformed As K-edge EXAFS
477 spectra of select FeEC and ACAIE samples and reference spectra with
478 the output of the shell-by-shell fits overlain on the data. The results of
479 the shell-by-shell fits are given in Table S2. For the FeEC sample at
480 CDR of 60 C/L/min, which was determined to be >95% As(III) by XANES
481 LCFs, the first-shell fits were consistent with As(III) based on the fit-
482 derived coordination number (CN_{As-O}) of 3.1 ± 0.4 and interatomic
483 distance (R_{As-O}) of $1.77 \pm 0.01 \text{ \AA}$.⁴⁸ The second shell of this sample was
484 fit with an As-Fe path with $CN = 1.3 \pm 0.6$ and $R = 3.41 \pm 0.03 \text{ \AA}$. This
485 R_{As-Fe} value is identical within fit-derived errors to previous studies
486 assigning this interatomic distance to As(III) bound in a binuclear
487 corner-sharing (²C) geometry to GR particle edges.⁴⁰ However, we note
488 that the fit-derived CN_{As-Fe} value of 1.3 ± 0.6 is slightly lower than the
489 theoretical value of 2.0 for the ²C geometry. Attempts to fit the second
490 shell with an As-Fe mononuclear edge-sharing (²E) bond with R_{As-Fe} near
491 3.0 \AA , which has been proposed in previous studies of As(III) bound to
492 Fe precipitates,⁴⁸ were unsuccessful, yielding physically meaningless
493 (or negative) values of CN_{As-Fe} and R_{As-Fe} .

494 Fits of the first and second shells of the solids formed in the
495 ACAIE system at CDR of 6 and 60 C/L/min were similar, indicating a
496 similar arsenic uptake mode regardless of CDR. The first shell As-O
497 parameters returned by the fit were CN_{As-O} of 4.4 ± 0.5 to 4.7 ± 0.5 and

498 $R_{\text{As-O}}$ of $1.69 \pm 0.01 \text{ \AA}$, consistent with As(V) in tetrahedral
499 coordination.⁴⁹ The second-shell fits in the ACAIE system yielded values
500 of 3.0 ± 0.8 to 3.1 ± 0.8 for $\text{CN}_{\text{As-Fe}}$ and $3.24 \pm 0.02 \text{ \AA}$ for $R_{\text{As-Fe}}$. These
501 second-shell fitting parameters are similar to those of the reference
502 spectrum of As(V) adsorbed to 2LFh ($\text{CN}_{\text{As-Fe}} = 1.9 \pm 0.9$; $R_{\text{As-Fe}} = 3.28 \pm$
503 0.03 \AA), but the ACAIE samples have a slightly higher CN. Based on
504 the $R_{\text{As-Fe}}$ of 3.24 \AA for ACAIE samples, we conclude that As(V) is bound
505 to the ACAIE solids in the ^2C geometry.⁴⁹ The $R_{\text{As-Fe}}$ of the ACAIE
506 samples (3.24 \AA) is almost 0.2 \AA shorter than the $R_{\text{As-Fe}}$ of the FeEC
507 sample at CDR of 60 C/L/min (3.41 \AA), which we identified as As(III)
508 bound also in the ^2C geometry. This difference in $R_{\text{As-Fe}}$ for the same ^2C
509 geometry reflects the shorter As-O distance of As(V) (1.69 \AA) compared
510 to As(III) (1.77 \AA) and the shorter average Fe-O distance (2.0 \AA) for
511 Fe(III) precipitates⁵⁰ compared to GR (2.1 \AA).⁵¹

512 **3.4 Field performance of a flow through ACAIE in rural** 513 **California**

514 Figure S7 shows the arsenic removal performance of the
515 continuous flow ACAIE system that treated 100 L (250 equivalent
516 reactor volumes, 19 second retention time) of real groundwater
517 followed by coagulation and flocculation. Pre-coagulation filtered
518 samples, collected during electrolysis, had a pale-yellow color
519 indicative of particulate Fe, which suggests arsenic-bearing Fe(III)
520 precipitates of sizes smaller than $0.45 \mu\text{m}$ passed through the filter.

521 Therefore, we measured dissolved iron concentrations above 0.3 mg/L
522 (WHO-SMCL) during electrolysis. Dissolved iron reached below 0.3 mg/
523 L after coagulation and flocculation with alum (5 mg/L as Al).
524 Dissolved arsenic concentrations decreased dramatically from an initial
525 value of 118 $\mu\text{g/L}$ to less than 30 $\mu\text{g/L}$ in the first five minutes and then
526 remained below 20 $\mu\text{g/L}$, when collected during electrolysis. After
527 flocculation, dissolved arsenic decreased to below 0.5 $\mu\text{g/L}$.

528 **4 Discussions**

529 **4.1 Impact of CDR on the structure of Fe precipitates in the** 530 **FeEC and ACAIE systems**

531 In FeEC, complete oxidation of Fe(II) to Fe(III) is achieved when
532 the rate of Fe(II) generation is less than rate of atmospheric O_2
533 dissolution; this typically occurs at low CDR. At a low CDR of 1.5
534 C/L/min, completely oxidized Fe(III) precipitates formed in FeEC, which
535 is consistent with the final DO near 3.5 mg/L (Figure S3B). At increased
536 CDR, measurements of the final DO below 0.1 mg/L indicate that the
537 rate of Fe(II) generation exceeded the rate of O_2 dissolution. This rapid
538 introduction of Fe(II) and consumption of DO at $\text{CDR} \geq 6$ C/L/min
539 resulted in incomplete Fe(II) oxidation and the formation of GR. This
540 conclusion is supported by the XRD and Fe K-edge XAS data as well as
541 the characteristic color of solids.

542 In contrast to the FeEC system, complete oxidation of Fe(II) to
543 Fe(III) during ACAIE treatment occurred due to the nearly equimolar

544 generation of H₂O₂ by the cathode, especially at high CDR (80-85%
545 efficiency, Figure S6).²⁶ In addition, the H₂O₂ Faradaic efficiency
546 remained nearly constant (~85 %) even when the CDR increased an
547 order of magnitude (from 60 to 600 C/L/min), which suggests negligible
548 O₂ diffusion limitations to the air cathode. The efficient production of
549 H₂O₂, which oxidizes Fe(II) at nearly 4 orders of magnitude faster than
550 DO,^{27, 28} explains why dissolved Fe(II) did not accumulate and GR did
551 not form in the ACAIE system even at the highest CDR of 1200 C/L/min.
552 While no transition from Fe(III) precipitates to GR was observed at in
553 the ACAIE system, some systematic changes in Fe(III) precipitate
554 structure with CDR were detected in the XRD data. At the lowest CDR
555 of 1.5 C/L/min, lepidocrocite was observed in the XRD, but 2LFh
556 became dominant as the CDR increased. This trend in reduced
557 crystallinity can be explained by the decreased efficiency of H₂O₂
558 production (48 ± 9% of the theoretical value) at CDR of 1.5 C/L/min
559 compared to the high efficiency of H₂O₂ production at CDR > 6 C/L/min.
560 Since <60% of the theoretical H₂O₂ was produced at CDR of 1.5
561 C/L/min, the half-life of Fe(II) in experiments at low CDR is likely longer
562 than at high CDR. The higher stability of Fe(II) at low CDR is consistent
563 with the well-documented rapid transformation of freshly-formed Fe(III)
564 precipitates to lepidocrocite catalyzed by Fe(II).^{52, 53} Another
565 speculative explanation for the difference in the structure of the Fe(III)
566 (oxyhydr)oxides is that long electrolysis times (~6.7 hours) at low CDR

567 of 1.5 C/L/min could allow sufficient time for crystallization of poorly-
568 ordered Fe(III) (oxyhydr)oxides to lepidocrocite by other crystal growth
569 mechanisms (e.g. oriented aggregation or Ostwald ripening).⁵⁴

570 **4.2 Behavior of arsenic in the FeEC and ACAIE systems**

571 In the FeEC experiments, we observed excellent removal of
572 As(III) to below 2 $\mu\text{g/L}$ at the lowest CDR of 1.5 C/L/min (Figure 1A). At
573 this CDR, we also observed the formation of strictly Fe(III)-bearing
574 solids. This effective arsenic removal is explained by complete
575 oxidation of Fe(II) by DO at low rates of Fe(II) addition, which leads to
576 As(III) outcompeting Fe(II) for Fe(IV), resulting in efficient As(III)
577 oxidation and removal.^{13, 34, 55} By contrast, as the CDR increased above
578 6 C/L/min in the FeEC system, we observed nearly 300 $\mu\text{g/L}$ of arsenic,
579 70 mg/L of Fe and <0.1 mg/L of DO remaining in the solution after
580 electrolysis (Figure 1, Figure S3B). In addition, our structural data
581 revealed the formation of GR. The lower arsenic removal efficiency at
582 high CDR in the FeEC system results from several processes related to
583 the increased Fe(II) addition rate. At high rates of Fe(II) addition, DO is
584 consumed rapidly and leads to the accumulation of aqueous Fe(II),
585 which outcompetes As(III) for reactive Fenton-type oxidants, resulting
586 in inefficient As(III) oxidation. This result is consistent with the As K-
587 edge XANES analysis showing the predominance of sorbed As(III) at
588 CDR >6 C/L/min (Figure 4). In addition, the formation of GR at high
589 CDRs likely decreases arsenic removal efficiency because of its lower

590 specific surface area compared to Fe(III) precipitates and GR could
591 compete with As(III) for the reactive oxidants.⁵⁶ Although we still
592 detected inner-sphere As(III) adsorption complexes on GR in the FeEC
593 experiments, our observation that GR did not remove arsenic
594 effectively is consistent with previous work showing Fe(III) precipitates
595 to be more advantageous to arsenic removal.³⁸

596 In contrast to the FeEC system, nearly 100% arsenic removal
597 was observed in ACAIE experiments at all CDRs. For example, aqueous
598 arsenic levels decreased from 1464 $\mu\text{g/L}$ to $<4 \mu\text{g/L}$, despite the 800-
599 fold shorter treatment time (400 to 0.5 minute electrolysis time for
600 CDR of 1.5 to 1200 C/L/min). In addition, we found no evidence for the
601 accumulation of Fe(II) nor the formation of GR in the ACAIE
602 experiments. The remarkable arsenic removal efficiency of the ACAIE
603 system results can be explained by the rapid kinetics of Fe(II) oxidation
604 by H_2O_2 coupled with higher yields of reactive oxidants. Despite air
605 saturated DO levels observed in the ACAIE system at all dosage rates
606 (Figure S3B), we expect H_2O_2 to outcompete DO to oxidize aqueous
607 Fe(II) ($k_{\text{app_H}_2\text{O}_2} = 10^{4.5} \text{ M}^{-1}\text{s}^{-1}$; $k_{\text{app_O}_2} = 10^{0.9} \text{ M}^{-1}\text{s}^{-1}$) because it reacts
608 quicker than DO. We validated this hypothesis with an additional
609 experiment provided in SI (Section S6, Figure S11). The more effective
610 production of reactive oxidants in the ACAIE system is consistent with
611 the As K-edge XANES and EXAFS data, which identified only As(V)
612 bound in the ^{23}C adsorption geometry to Fe(III) precipitate surfaces,

613 regardless of CDR. In addition to efficient oxidation of As(III) to As(V),
614 the lower crystallinity of Fe(III) (oxyhydr)oxides compared to GR
615 formed at high CDR can also benefit arsenic removal because of their
616 high specific surface area.

617 **4.3 Electrolyte composition**

618 Comparing the laboratory experiments, which were conducted
619 primarily in SBGW, with the field experiments performed in real
620 groundwater allows us to examine the influence of groundwater
621 chemistry on arsenic removal in the ACAIE system. For example,
622 previous studies indicate that Ca and Mg aid in the aggregation and
623 flocculation of Fe(III) (oxyhydr)oxides by charge neutralization.^{57, 58}
624 Consequently, in the laboratory experiments, high concentrations of Ca
625 and Mg in SBGW likely aided the aggregation of the solids (nominal
626 diameter >0.45 μ m), resulting in effective particle removal by filtering
627 with measurements of iron and arsenic in the filtered solutions below
628 their respective SMCL and MCL. However, low concentrations of Ca and
629 Mg in Allensworth groundwater prevented the aggregation of Fe(III)
630 (oxyhydr)oxides (nominal size around 0.45 μ m), which lead to some of
631 the arsenic-rich Fe(III) (oxyhydr)oxides passing the filters.⁵⁹ This was
632 evident by the yellow color of the filtered samples and measurements
633 of arsenic in the filtered solution above the WHO-MCL during
634 electrolysis. However, the addition of alum at the end of electrolysis in
635 the field experiments resulted in the particle flocculation and dissolved

636 iron and arsenic remained far below their respective SMCLs of 0.3 mg/L
637 and 10 µg/L respectively. Dissolved organic carbon in the groundwater
638 could also be responsible for the poor aggregation of Fe(III)
639 (oxyhydr)oxides generated in the field. These results confirm the
640 importance of solution composition (e.g., bivalent cations, dissolved
641 organic carbon) for the removal of particulate iron by filtration.
642 Therefore, an additional coagulation and flocculation step is
643 recommended for particle separation. However, recent studies show
644 that electrocoagulation systems could be coupled with membrane
645 filtration to further decrease treatment times compared to
646 gravitational settling.⁶⁰⁻⁶²

647 **4.4 Technical and environmental implications**

648 Recent studies show that arsenic levels even below 10 µg/L can
649 cause significant increases in excess cancers, which calls for
650 innovative treatment solutions that can remove arsenic to <1 µg/L.⁶³
651 Our results show that ACAIE can achieve arsenic removal <1 µg/L at
652 CDRs of 1.5 and 6 C/L/min. At higher CDRs (and shorter treatment
653 duration) 1 µg/L arsenic can be likely achieved by increasing and
654 optimizing the total charge dose, which is currently under investigation
655 in our laboratory. In addition, ACAIE removes arsenic to <4 µg/L with
656 superior energy efficiency than that of FeEC (Figure S9). The reduction
657 in Electrical Energy per Order for ACAIE, relative to FeEC, ranges from
658 8% to 76% between CDRs 1.5 to 600 C/L/min (Figure S9). Therefore,

659 target arsenic levels of $<1 \mu\text{g/L}$ can likely be achieved at significantly
660 lower operating costs with ACAIE relative to FeEC. Furthermore, the
661 extremely short treatment duration (i.e. short residence time) implies
662 that ACAIE systems require a much smaller footprint than an
663 equivalent FeEC system. This also could lead to smaller capital cost for
664 the reactor. Based on these benefits, we propose that ACAIE can be a
665 breakthrough technology to decrease arsenic concentrations to less
666 than $<1 \mu\text{g/L}$ both in large-scale water treatment plants in rural
667 communities relying on decentralized treatment.

668 Importantly, the As K-edge XANES and EXAFS spectra showed
669 that the bonding environment of As(V) did not change with CDR in the
670 ACAIE system, with As(V) forming the ^2C adsorption complex with
671 Fe(III) (oxyhydr)oxides in all experiments. Given the wide range of
672 electrolysis times, detection of the same ^2C adsorption complex is
673 remarkable. This result is also important since the As and Fe bonding
674 environment in the reaction products of the ACAIE system are nearly
675 identical to arsenic-rich Fe(III) precipitates that have been tested
676 previously for arsenic leachability by the Toxicity Characteristic
677 Leaching Procedure (TCLP)^{55, 64} and for long-term disposal by
678 incorporation in concrete.^{65, 66} Therefore, the results of previous
679 investigations of the fate of arsenic-rich Fe(III) precipitates during
680 sludge storage and disposal will likely be applicable to the ACAIE

681 treatment residuals, which is useful to inform sludge management
682 strategies.

683 Low mechanical stability of large size air cathodes could limit the
684 scale-up of ACAIE for single-size very large treatment systems. While
685 mechanical stability can be a concern for single air cathodes of very
686 large size (e.g. larger than a square meter), our field experiments were
687 performed with a modestly large air cathode assembly (air cathode of
688 400 cm²) and showed mechanical stability and high efficiency for
689 extended periods. Furthermore, when targeting rural, decentralized
690 communities, small scale ACAIE systems can be implemented with
691 vertically stacked multiple ACAIE reactors, each of moderate scale,
692 without resorting to very large electrodes. However, if eventually
693 larger electrodes are required for much higher capacity ACAIE systems
694 than those in our field tests, screen printing techniques can be
695 explored to fabricate air cathodes with several m² surface.

696 Finally, fouling of the air cathodes can be caused by the
697 precipitation of Ca and Mg carbonates due to local regions of alkaline
698 pH near the cathodes²⁶ and by the physical accumulation of Fe(III)
699 (oxyhydr)oxides on the cathode surface over months to years of
700 operation. However, we observed no significant change in cathodic
701 H₂O₂ production in waters containing high Ca and Mg concentrations
702 (Figure S10), consistent with previous findings.²⁶ We note that the
703 impact of fouling by Fe(III) (oxyhydr)oxides on the cathode over long-

704 term continuous operation, which could decrease H₂O₂ production,
705 should be investigated to increase the operational life of the cathodes.

706

707 **Supporting Information**

708 The supporting information contains: SBGW recipe, air cathode
709 fabrication, Faradaic efficiency of H₂O₂ measurements, energy
710 consumption data, controlled experiments to test the dominant oxidant
711 in ACAIE, X-ray absorption spectroscopy details, long-term
712 performance of the air cathode, in addition to supporting tables and
713 figures referenced in the main manuscript. The supporting information
714 is available free of charge via the internet at <http://pubs.acs.org>.

715

716 **Acknowledgements**

717 We acknowledge funding support from Andrew and Virginia Rudd
718 Family Foundation Chair Funds of Prof. Gadgil, CHED funded PCARI
719 project at UC Berkeley, TRDRP project administered by UCOP (Grant no
720 T29IR0649), CERC-WET project supported by the US Department of
721 Energy under award No.DE-IA0000018 at UC Berkeley, Dr. Gadgil's gift
722 funds at LBNL. Synchrotron experiments were performed at SSRL,
723 SLAC National Accelerator Laboratory supported by the U.S.
724 Department of Energy, Office of Science, Basic Energy Sciences, under
725 Contract No. DE-AC02-76SF00515. XRD experiments were performed
726 at Molecular Foundry, LBNL, supported by the Office of Basic Energy

727 Sciences of the U.S. DOE under Contract No. DE-AC02-05CH11231. We
728 sincerely thank the anonymous reviewers whose comments have
729 improved this manuscript. We are also grateful to James Barazesh,
730 Yanghua Duan, Rachel Scholes and Marc Teixido Planes for valuable
731 discussions and help. Authors are thankful to Jacob Gallego and Jeff
732 Higginbotham from the mechanical engineering student machine shop
733 for their high-quality assistance in the fabrication of ACAIE reactors.
734 SRSB gratefully acknowledges support from CEE Department Block
735 Grant and CEE Nanotechnology Fellowship. SG and DH are grateful for
736 NSF-GRFP Fellowship support.

737 **References**

- 738 1. Naujokas, M. F.; Anderson, B.; Ahsan, H.; Aposhian, H. V.;
739 Graziano, J. H.; Thompson, C.; Suk, W. A., The Broad Scope of Health
740 Effects from Chronic Arsenic Exposure: Update on a Worldwide Public
741 Health Problem. *Environ Health Persp* **2013**, *121*, (3), 295-302.
- 742 2. Murcott, S., *Arsenic contamination in the world*. IWA publishing:
743 2012.
- 744 3. Steinmaus, C. M.; Ferreccio, C.; Romo, J. A.; Yuan, Y.; Cortes, S.;
745 Marshall, G.; Moore, L. E.; Balmes, J. R.; Liaw, J.; Golden, T.; Smith, A.
746 H., Drinking water arsenic in northern chile: high cancer risks 40 years
747 after exposure cessation. *Cancer Epidemiol Biomarkers Prev* **2013**, *22*,
748 (4), 623-30.
- 749 4. Smith, A. H.; Lopipero, P. A.; Bates, M. N.; Steinmaus, C. M.,
750 Public health - Arsenic epidemiology and drinking water standards.
751 *Science* **2002**, *296*, (5576), 2145-2146.
- 752 5. Smith, A. H.; Hopenhayn-Rich, C.; Bates, M. N.; Goeden, H. M.;
753 Hertz-Picciotto, I.; Duggan, H. M.; Wood, R.; Kosnett, M. J.; Smith, M. T.,
754 Cancer risks from arsenic in drinking water. *Environ Health Perspect*
755 **1992**, *97*, 259-67.
- 756 6. Chakraborti, D.; Rahman, M. M.; Chatterjee, A.; Das, D.; Das, B.;
757 Nayak, B.; Pal, A.; Chowdhury, U. K.; Ahmed, S.; Biswas, B. K.;
758 Sengupta, M. K.; Lodh, D.; Samanta, G.; Chakraborty, S.; Roy, M. M.;
759 Dutta, R. N.; Saha, K. C.; Mukherjee, S. C.; Pati, S.; Kar, P. B., Fate of
760 over 480 million inhabitants living in arsenic and fluoride endemic

- 761 Indian districts: Magnitude, health, socio-economic effects and
762 mitigation approaches. *J Trace Elem Med Bio* **2016**, *38*, 33-45.
- 763 7. Johnston, R. B.; Hanchett, S.; Khan, M. H., The socio-economics of
764 arsenic removal. *Nat Geosci* **2010**, *3*, (1), 2-3.
- 765 8. Amrose, S.; Burt, Z.; Ray, I., Safe Drinking Water for Low-Income
766 Regions. *Annu Rev Env Resour* **2015**, *40*, 203-231.
- 767 9. Kumar, P. R.; Chaudhari, S.; Khilar, K. C.; Mahajan, S. P., Removal
768 of arsenic from water by electrocoagulation. *Chemosphere* **2004**, *55*,
769 (9), 1245-1252.
- 770 10. Hernandez, D.; Boden, K.; Paul, P.; Bandaru, S.; Mypati, S.; Roy,
771 A.; Amrose, S.; Roy, J.; Gadgil, A., Strategies for successful field
772 deployment in a resource-poor region: Arsenic remediation technology
773 for drinking water. *Development Engineering* **2019**, *4*, 100045.
- 774 11. Amrose, S. E.; Bandaru, S. R. S.; Delaire, C.; van Genuchten, C.
775 M.; Dutta, A.; DebSarkar, A.; Orr, C.; Roy, J.; Das, A.; Gadgil, A. J.,
776 Electro-chemical arsenic remediation: Field trials in West Bengal. *Sci*
777 *Total Environ* **2014**, *488*, 543-550.
- 778 12. Lakshmanan, D.; Clifford, D. A.; Samanta, G., Ferrous and Ferric
779 Ion Generation During Iron Electrocoagulation. *Environ Sci Technol*
780 **2009**, *43*, (10), 3853-3859.
- 781 13. Hug, S. J.; Leupin, O., Iron-catalyzed oxidation of arsenic(III) by
782 oxygen and by hydrogen peroxide: pH-dependent formation of
783 oxidants in the Fenton reaction. *Environ Sci Technol* **2003**, *37*, (12),
784 2734-2742.
- 785 14. Roberts, L. C.; Hug, S. J.; Ruettimann, T.; Billah, M.; Khan, A. W.;
786 Rahman, M. T., Arsenic removal with iron(II) and iron(III) in waters with
787 high silicate and phosphate concentrations. *Environ Sci Technol* **2004**,
788 *38*, (1), 307-15.
- 789 15. Lu, H. F.; Chen, H. F.; Kao, C. L.; Chao, I.; Chen, H. Y., A
790 computational study of the Fenton reaction in different pH ranges.
791 *Phys Chem Chem Phys* **2018**, *20*, (35), 22890-22901.
- 792 16. Wiegand, H. L.; Orths, C. T.; Kerpen, K.; Lutze, H. V.; Schmidt, T.
793 C., Investigation of the Iron-Peroxo Complex in the Fenton Reaction:
794 Kinetic Indication, Decay Kinetics, and Hydroxyl Radical Yields. *Environ*
795 *Sci Technol* **2017**, *51*, (24), 14321-14329.
- 796 17. Bataineh, H.; Pestovsky, O.; Bakac, A., pH-induced mechanistic
797 changeover from hydroxyl radicals to iron(IV) in the Fenton reaction.
798 *Chem Sci* **2012**, *3*, (5), 1594-1599.
- 799 18. Delaire, C.; Amrose, S.; Zhang, M. H.; Hake, J.; Gadgil, A., How do
800 operating conditions affect As(III) removal by iron electrocoagulation?
801 *Water Res* **2017**, *112*, 185-194.
- 802 19. van Genuchten, C. M.; Behrends, T.; Stipp, S. L. S.; Dideriksen, K.,
803 Achieving arsenic concentrations of <1mg/L by Fe(0) electrolysis: The
804 exceptional performance of magnetite. *Water Res* **2020**, *168*, 115170.

- 805 20. Dubrawski, K. L.; van Genuchten, C. M.; Delaire, C.; Amrose, S.
806 E.; Gadgil, A. J.; Mohseni, M., Production and Transformation of Mixed-
807 Valent Nanoparticles Generated by Fe(0) Electrocoagulation. *Environ*
808 *Sci Technol* **2015**, *49*, (4), 2171-2179.
- 809 21. van Genuchten, C. M.; Behrends, T.; Kraal, P.; Stipp, S. L. S.;
810 Dideriksen, K., Controls on the formation of Fe(II,III) (hydr)oxides by
811 Fe(0) electrolysis. *Electrochim Acta* **2018**, *286*, 324-338.
- 812 22. Jiang, Y. Y.; Ni, P. J.; Chen, C. X.; Lu, Y. Z.; Yang, P.; Kong, B.;
813 Fisher, A.; Wang, X., Selective Electrochemical H₂O₂ Production
814 through Two-Electron Oxygen Electrochemistry. *Adv Energy Mater*
815 **2018**, *8*, (31), 1801909.
- 816 23. Rozendal, R. A.; Leone, E.; Keller, J.; Rabaey, K., Efficient
817 hydrogen peroxide generation from organic matter in a
818 bioelectrochemical system. *Electrochem Commun* **2009**, *11*, (9), 1752-
819 1755.
- 820 24. Xia, C.; Xia, Y.; Zhu, P.; Fan, L.; Wang, H., Direct electrosynthesis
821 of pure aqueous H₂O₂ solutions up to 20% by weight using a solid
822 electrolyte. *Science* **2019**, *366*, (6462), 226-231.
- 823 25. Cheng, S.; Liu, H.; Logan, B. E., Increased performance of single-
824 chamber microbial fuel cells using an improved cathode structure.
825 *Electrochem Commun* **2006**, *8*, (3), 489-494.
- 826 26. Barazesh, J. M.; Hennebel, T.; Jasper, J. T.; Sedlak, D. L., Modular
827 Advanced Oxidation Process Enabled by Cathodic Hydrogen Peroxide
828 Production. *Environ Sci Technol* **2015**, *49*, (12), 7391-7399.
- 829 27. King, D. W.; Farlow, R., Role of carbonate speciation on the
830 oxidation of Fe(II) by H₂O₂. *Mar Chem* **2000**, *70*, (1-3), 201-209.
- 831 28. King, D. W., Role of carbonate speciation on the oxidation rate of
832 Fe(II) in aquatic systems. *Environ Sci Technol* **1998**, *32*, (19), 2997-
833 3003.
- 834 29. Si, Y. X.; Li, G. H.; Zhang, F., Energy-Efficient Oxidation and
835 Removal of Arsenite from Groundwater Using Air-Cathode Iron
836 Electrocoagulation. *Environ Sci Tech Let* **2017**, *4*, (2), 71-75.
- 837 30. Hering, J. G.; Katsoyiannis, I. A.; Theoduloz, G. A.; Berg, M.; Hug,
838 S. J., Arsenic Removal from Drinking Water: Experiences with
839 Technologies and Constraints in Practice. *J Environ Eng* **2017**, *143*, (5),
840 03117002.
- 841 31. Dixit, S.; Hering, J. G., Comparison of arsenic(V) and arsenic(III)
842 sorption onto iron oxide minerals: Implications for arsenic mobility.
843 *Environ Sci Technol* **2003**, *37*, (18), 4182-4189.
- 844 32. Huhmann, B. L.; Neumann, A.; Boyanov, M. I.; Kemner, K. M.;
845 Scherer, M. M., Emerging investigator series: As(v) in magnetite:
846 incorporation and redistribution. *Environ Sci-Proc Imp* **2017**, *19*, (10),
847 1208-1219.
- 848 33. Delaire, C.; van Genuchten, C. M.; Nelson, K. L.; Amrose, S. E.;
849 Gadgil, A. J., Escherichia coli Attenuation by Fe Electrocoagulation in

- 850 Synthetic Bengal Groundwater: Effect of pH and Natural Organic
851 Matter. *Environ Sci Technol* **2015**, *49*, (16), 9945-9953.
- 852 34. Li, L.; van Genuchten, C. M.; Addy, S. E. A.; Yao, J. J.; Gao, N. Y.;
853 Gadgil, A. J., Modeling As(III) Oxidation and Removal with Iron
854 Electrocoagulation in Groundwater. *Environ Sci Technol* **2012**, *46*, (21),
855 12038-12045.
- 856 35. Hansen, H. C. B., Composition, Stabilization, and Light-Absorption
857 of Fe(II)Fe(III) Hydroxy-Carbonate (Green Rust). *Clay Miner* **1989**, *24*,
858 (4), 663-669.
- 859 36. Webb, S., SIXPACK: a graphical user interface for XAS analysis
860 using IFEFFIT. *Physica Scripta* **2005**, *T115*, 1011-1014.
- 861 37. van Genuchten, C.; Addy, S.; Pena, J.; Gadgil, A., Removing
862 arsenic from synthetic groundwater with iron electrocoagulation: An Fe
863 and As K-edge EXAFS study. *Environmental Science & Technology*
864 **2012**, *46*, (2), 986-994.
- 865 38. van Genuchten, C. M.; Behrends, T.; Dideriksen, K., Emerging
866 investigator series: interdependency of green rust transformation and
867 the partitioning and binding mode of arsenic. *Environ Sci Process*
868 *Impacts* **2019**, *21*, (9), 1459-1476.
- 869 39. Newville, M., IFEFFIT: interactive XAFS analysis and FEFF fitting. *J*
870 *Synchrotron Radiat* **2001**, *8*, (Pt 2), 322-4.
- 871 40. Jonsson, J.; Sherman, D. M., Sorption of As(III) and As(V) to
872 siderite, green rust (fougerite) and magnetite: Implications for arsenic
873 release in anoxic groundwaters. *Chem Geol* **2008**, *255*, (1-2), 173-181.
- 874 41. Rehr, J. J.; Albers, R. C.; Zabinsky, S. I., High-order multiple-
875 scattering calculations of x-ray-absorption fine structure. *Phys Rev Lett*
876 **1992**, *69*, (23), 3397-3400.
- 877 42. Kitahama, K.; Kiriya, R.; Baba, Y., Refinement of Crystal-
878 Structure of Scorodite. *Acta Crystallogr B* **1975**, *31*, (Jan15), 322-324.
- 879 43. Downs, R. T.; Hall-Wallace, M., The American Mineralogist crystal
880 structure database. *American Mineralogist* **2003**, *88*, (1), 247-250.
- 881 44. Ruby, C.; Usman, M.; Naille, S.; Hanna, K.; Carteret, C.; Mullet,
882 M.; Francois, M.; Abdelmoula, M., Synthesis and transformation of iron-
883 based layered double hydroxides. *Appl Clay Sci* **2010**, *48*, (1-2), 195-
884 202.
- 885 45. Liu, A. R.; Liu, J.; Pan, B. C.; Zhang, W. X., Formation of
886 lepidocrocite (γ -FeOOH) from oxidation of nanoscale zero-valent
887 iron (nZVI) in oxygenated water. *Rsc Adv* **2014**, *4*, (101), 57377-
888 57382.
- 889 46. Su, C. M.; Wilkin, R. T., Arsenate and arsenite sorption on and
890 arsenite oxidation by iron(II, III) hydroxycarbonate green rust. *Acs Sym*
891 *Ser* **2005**, *915*, 25-40.
- 892 47. Voegelin, A.; Kaegi, R.; Frommer, J.; Vantelon, D.; Hug, S. J.,
893 Effect of phosphate, silicate, and Ca on Fe(III)-precipitates formed in

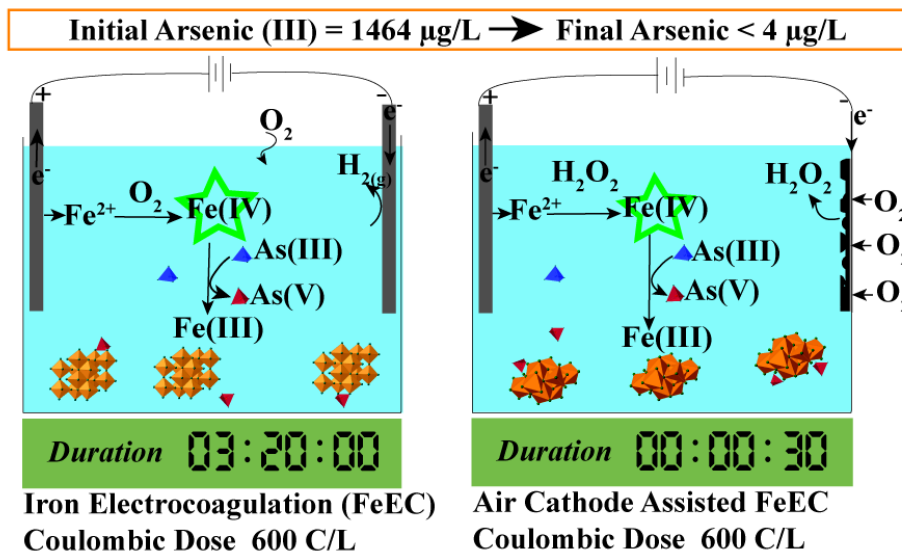
- 894 aerated Fe(II)- and As(III)-containing water studied by X-ray absorption
895 spectroscopy. *Geochim Cosmochim Acta* **2010**, *74*, (1), 164-186.
- 896 48. Ona-Nguema, G.; Morin, G.; Juillot, F.; Calas, G.; Brown, G. E.,
897 EXAFS analysis of arsenite adsorption onto two-line ferrihydrite,
898 hematite, goethite, and lepidocrocite. *Environ Sci Technol* **2005**, *39*,
899 (23), 9147-9155.
- 900 49. Waychunas, G. A.; Rea, B. A.; Fuller, C. C.; Davis, J. A., Surface-
901 chemistry of ferrihydrite .1. Exafs studies of the geometry of
902 coprecipitated and adsorbed arsenate. *Geochim Cosmochim Acta* **1993**,
903 *57*, (10), 2251-2269.
- 904 50. Michel, F. M.; Ehm, L.; Antao, S. M.; Lee, P. L.; Chupas, P. J.; Liu,
905 G.; Strongin, D. R.; Schoonen, M. A. A.; Phillips, B. L.; Parise, J. B., The
906 structure of ferrihydrite, a nanocrystalline material. *Science* **2007**,
907 *316*, (5832), 1726-1729.
- 908 51. Trolard, F.; Bourrie, G.; Abdelmoula, M.; Refait, P.; Feder, F.,
909 Fougérite, a new mineral of the pyroaurite-iowaite group: Description
910 and crystal structure. *Clay Clay Miner* **2007**, *55*, (3), 323-334.
- 911 52. Pedersen, H.; Postma, D.; Jakobsen, R.; Larsen, O., Fast
912 transformation of iron oxyhydroxides by the catalytic action of aqueous
913 Fe(II). *Geochim Cosmochim Acta* **2005**, *69*, (16), 3967-3977.
- 914 53. Liu, H.; Li, P.; Zhu, M.; Wei, Y.; Sun, Y., Fe(II)-induced
915 transformation from ferrihydrite to lepidocrocite and goethite. *Journal*
916 *of Solid State Chemistry* **2007**, *180*, (7), 2121-2128.
- 917 54. Cornell, R. M.; Schwertmann, U., *The iron oxides: structure,*
918 *properties, reactions, occurrences and uses*. John Wiley & Sons: 2003.
- 919 55. Amrose, S.; Gadgil, A.; Srinivasan, V.; Kowolik, K.; Muller, M.;
920 Huang, J.; Kosteki, R., Arsenic removal from groundwater using iron
921 electrocoagulation: Effect of charge dosage rate. *J Environ Sci Heal A*
922 **2013**, *48*, (9), 1019-1030.
- 923 56. Usman, M.; Abdelmoula, M.; Hanna, K.; Gregoire, B.; Faure, P.;
924 Ruby, C., Fe-II induced mineralogical transformations of ferric
925 oxyhydroxides into magnetite of variable stoichiometry and
926 morphology. *Journal of Solid State Chemistry* **2012**, *194*, 328-335.
- 927 57. Zhang, Y. Y.; She, X. W.; Gao, X.; Shan, C.; Pan, B. C.,
928 Unexpected Favorable Role of Ca²⁺ in Phosphate Removal by Using
929 Nanosized Ferric Oxides Confined in Porous Polystyrene Beads. *Environ*
930 *Sci Technol* **2019**, *53*, (1), 365-372.
- 931 58. van Genuchten, C. M.; Pena, J.; Amrose, S. E.; Gadgil, A. J.,
932 Structure of Fe(III) precipitates generated by the electrolytic dissolution
933 of Fe(0) in the presence of groundwater ions. *Geochim Cosmochim Acta*
934 **2014**, *127*, 285-304.
- 935 59. van Genuchten, C. M.; Gadgil, A. J.; Pena, J., Fe(III) Nucleation in
936 the Presence of Bivalent Cations and Oxyanions Leads to Subnanoscale
937 7 angstrom Polymers. *Environ Sci Technol* **2014**, *48*, (20), 11828-
938 11836.

- 939 60. Ghurye, G.; Clifford, D.; Tripp, A., Iron coagulation and direct
940 microfiltration to remove arsenic from groundwater. *J Am Water Works*
941 *Ass* **2004**, *96*, (4), 143-152.
- 942 61. Zouboulis, A.; Katsoyiannis, I., Removal of arsenates from
943 contaminated water by coagulation-direct filtration. *Separ Sci Technol*
944 **2002**, *37*, (12), 2859-2873.
- 945 62. Ahmad, A.; Rutten, S.; de Waal, L.; Volvaard, P.; van Genuchten,
946 C.; Bruning, H.; Cornelissen, E.; van der Wal, A., Mechanisms of
947 arsenate removal and membrane fouling in ferric based
948 coprecipitation-low pressure membrane filtration systems. *Sep Purif*
949 *Technol* **2020**, *241*, 116644.
- 950 63. Ahmad, A.; van der Wens, P.; Baken, K.; de Waal, L.;
951 Bhattacharya, P.; Stuyfzand, P., Arsenic reduction to < 1 µg/L in Dutch
952 drinking water. *Environment International* **2020**, *134*, 105253.
- 953 64. Xie, S. W.; Yuan, S. H.; Liao, P.; Tong, M.; Gan, Y. Q.; Wang, Y. X.,
954 Iron-Anode Enhanced Sand Filter for Arsenic Removal from Tube Well
955 Water. *Environ Sci Technol* **2017**, *51*, (2), 889-896.
- 956 65. Roy, A.; van Genuchten, C. M.; Mookherje, I.; Debsarkar, A.;
957 Dutta, A., Concrete stabilization of arsenic-bearing iron sludge
958 generated from an electrochemical arsenic remediation plant. *J Environ*
959 *Manage* **2019**, *233*, 141-150.
- 960 66. Clancy, T. M.; Snyder, K. V.; Reddy, R.; Lanzirrotti, A.; Amrose, S.
961 E.; Raskin, L.; Hayes, K. F., Evaluating the cement stabilization of
962 arsenic-bearing iron wastes from drinking water treatment. *J Hazard*
963 *Mater* **2015**, *300*, 522-529.
- 964

965

966 **Figure FOR TABLE OF CONTENTS ONLY**

967



968